WILEY ONLINE LIBRARY

Early View publication on wileyonlinelibrary.com
(issue and page numbers not yet assigned;
citable using Digital Object Identifier – DOI)

LASER & PHOTONICS REVIEWS

Laser Photonics Rev., 1–15 (2012) / **DOI** 10.1002/lpor.201100029

Abstract InAs/(In,Ga)Sb Strained Layer Superlattices (SLSs) have made significant progress since they were first proposed as an infrared (IR) sensing material more than three decades ago. The basic material properties of SLS provide a prospective benefit in the realization of IR imagers with suppressed interband tunneling and Auger recombination processes, as well as high quantum efficiency and responsivity. With scaling of single pixel dimensions, the performance of focal plane arrays is strongly dependent on surface effects due to the large pixels' surface/volume ratio. This article discusses the cause of surface leakage currents and various approaches of their reduction including dielectric passivation, passivation with organic materials (polyimide or various photoresists), passivation by overgrowth of wider bandgap material, and chalcogenide passivation. Performance of SLS detectors passivated by different techniques and operating in various regions of infrared spectrum has been compared.

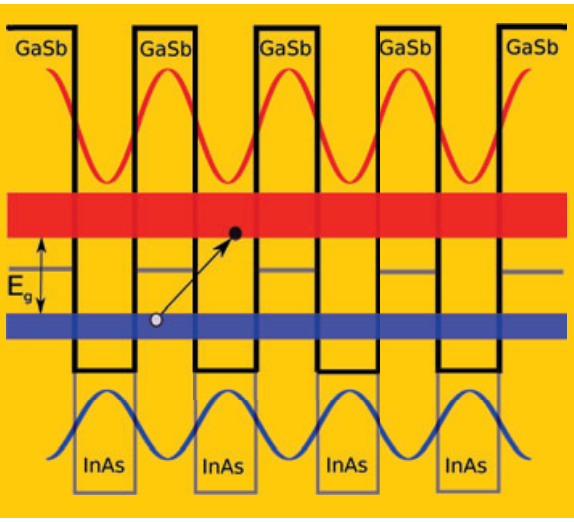

Passivation techniques for InAs/GaSb strained layer superlattice detectors

Elena A. Plis*, **Maya Narayanan Kutty, and Sanjay Krishna**

1. InAs/GaSb strained layer superlattice detectors in infrared detection technology

The InAs/(In,Ga)Sb strained layer superlattices (SLSs) were first proposed as an infrared (IR) sensing material in 1980s by Sai-Halasz, Tsu and Esaki [1, 2]. IR detectors based on InAs/(In,Ga)Sb SLSs have been investigated for the past several decades, ever since they were suggested by Smith and Malhiot for IR detection [3]. In 1990, Chow and coworkers first reported $Ga_{1-x}In_xSb$/InAs SLS material with high structural quality, long wave IR (LWIR) photoresponse, and LWIR photoluminescence [4].

The InAs/(In,Ga)Sb SLS material system is characterized by a broken-gap type-II alignment illustrated in Fig. 1 with electrons and holes localized in InAs and (In,Ga)Sb layers, respectively. The overlap of electron (hole) wave functions between adjacent InAs (InGaSb) layers results in the formation of an electron (hole) minibands in the conduction (valence) band. Optical transition between the highest hole (heavy-hole) and the lowest conduction minibands is employed for the detection of incoming IR radiation. The effective bandgap of the InAs/ (In,Ga)Sb SLSs can be tailored from 3 µm to 32 µm by varying thickness of constituent layers. While theoretical predictions seem to favor the InAs/InGaSb system due to the additional strain provided by the InGaSb layer, most of the experimental results in the past five years have been on the binary InAs/GaSb system. This is attributed to the complexity of structures grown with the large mole fraction of In. Several research

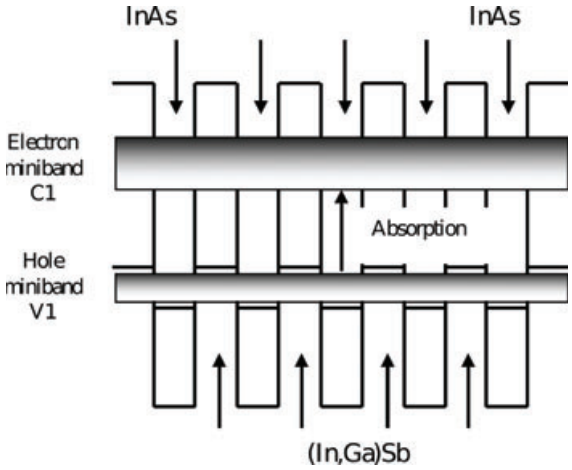

Figure 1 Absorption in InAs/(In,Ga)Sb SLS.

groups within the last years have reported on high performance InAs/GaSb SLS IR detectors and focal plane arrays (FPAs) for mid-wave IR (MWIR) [5–7], long-wave IR (LWIR) [8–12], and very-long wave (VLWIR) [13, 14] spectral regions.

Presently, most common IR materials that are used are bulk mercury cadmium telluride (MCT), InSb, and GaAs/AlGaAs quantum well (QW). MCT and InSb provide the state-of-the-art IR imaging cameras today [15–17]. Despite excellent performance in MWIR and LWIR spec-

Center for High Technology Materials, Electrical and Computer Engineering Department, University of New Mexico, Albuquerque, NM, 87106, USA
* Corresponding author: e-mail: a1ien@chtm.unm.edu

tral regions, the spatial non-uniformity over large area still plaques MCT material. Moreover, MCT is characterized by low electron effective mass resulting in excessive leakage current [18]. The InSb detectors do not cover the LWIR spectral range. The GaAs/AlGaAs QW material [19–21] benefits from mature III-V growth and processing capabilities, featuring commercially available, lattice-matched substrates for high-quality epitaxial growth. Relatively high values of thermally generated leakage current caused by electron tunneling between quantum wells limit the operating temperature of GaAs/AlGaAs QW - based devices to ~ 60 K. Moreover, due to polarization selection rules for electron-photon interactions GaAs/AlGaAs QW material is insensitive to surface-normal incident IR radiation resulting in poor conversion quantum efficiency.

By controlling the strain at the SLS interfaces, extremely thick (~ 6 µm, e.g. [22]) active regions can be grown resulting in a large quantum efficiency and responsivity of the SLS detectors. Tunneling currents in SLS are reduced due to larger electron effective mass. Large splitting between heavy-hole and light-hole valence subbands due to strain in the SLSs contributes to the suppression of Auger recombination [23, 24]. Moreover, the SLSs are less sensitive to the bandgap variations due to compositional non-uniformities than the MCT alloys with the same bandgap [25]. Finally, in contrast with QWIPs, normal incidence absorption is permitted in SLSs, contributing to high conversion quantum efficiency. Excellent comparisons of the MCT, InSb, QWIP and SLS technologies can be found in [26–28]

2. Limitations of SLS technology

SLS offer numerous advantages over present day detection technologies including reduced tunneling currents, normal incidence absorption and suppressed Auger recombination. Commercial availability of low defect density substrates as well as a high degree of uniformity for III-V growth and processing over a large area also offers technological advantages for the InAs/GaSb SLS technology.

A typical SLS FPA has pitch dimensions of 30 µm × 30 µm and involves the following fabrication steps: the individual pixel isolation and passivation; contact metalization followed by the under bump metal (UBM) deposition; bump metal (indium) deposition; reflow process, hybridization of FPA to the read-out integrated circuit (ROIC) and the substrate removal. There is an increased emphasis on large format (1 M–4 M) FPAs in which the pixel size is further shrunk to 15 µm × 15 µm.

During the individual pixel isolation process, the periodic crystal structure terminates abruptly resulting in formation of unsatisfied (dangling) chemical bonds responsible for generation of surface states within the bandgap. These states cause pinning of the surface Fermi level near the midgap and, as a consequence, enhance the surface leakage currents. Moreover, the surface leakage currents become a dominant contributor to the dark current for FPA pixels with mesa dimensions of ~ 20 µm. Thus, in order to improve the overall device performance, methods for elimination of surface currents, i.e. passivation treatments, have to be developed for InAs/GaSb SLS material system.

The FPA pixel dimensions and high fill factor give rise to problems of accurate mesa dimensions and edge definition control. Furthermore, passivation treatment applied to the etched surfaces that are rough, or contaminated by native oxides and foreign particles, will result in little or no improvement of device performance. Effective methods of native oxide removal or thinning have to be incorporated into the device fabrication sequence prior the passivation step.

The paper is organized as follows: first we will elaborate on the conductive nature of some of native oxides formed on exposed sidewalls of InAs/GaSb SLS detectors and common methods of native oxide reduction. Next, InAs/GaSb SLS mesa deliniation techniques will be reviewed including plasma assisted etch and chemical etch. Finally, various approaches to passivation of InAs/GaSb SLS detectors will be discussed including dielectric passivation, passivation with organic materials (polyimide or various photoresists), passivation by overgrowth of wider bandgap material, and chalcogenide passivation. Electrical performance of SLS detectors passivated by different techniques and operating in MWIR, LWIR, and VLWIR spectral regions will be presented.

3. Surface effects

There are three major components of dark current in detectors based on narrow band gap semiconductors.

1. Generation current associated with the Shockley-Read-Hall (SRH) process in the depletion region of the detector.
2. Thermally generated diffusion current associated with Auger [29] or radiative process in both the n- and p-extrinsic regions of the detector.
3. A surface current associated with the surface states in the junction.

With the SRH and thermally generated diffusion currents being greatly reduced by the intricated heterostructure engineering [9, 11], the surface current remains a dominant contributor to the total dark current. The performance of individual FPA pixels with typical mesa dimensions of ~ 20 µm × 20 µm is strongly dependent on surface effects due to their large surface/volume ratio.

The presence of surface leakage may be explained using the surface potential theory. With a nonzero surface potential at the sidewall interface, band-bending occurs due to the Fermi level position and this results in accumulation/inversion of majority carriers that then can create conductive leakage channels parallel to the surface.

The most important reasons for the nonzero surface potential are the abrupt termination of periodic crystalline lattice at the semiconductor-air interface with formation of unsatisfied (dangling) bonds and undulation effects presented on the device sidewalls due to differential etch rate of SLSs constituent layers (InAs, GaSb, InSb, GaAs, and sometimes AlSb). In addition to the surface potential modification native oxides and contaminants also contribute to

dark current by creating additional interfacial states. Interface states located within band-gap alleviate the carrier tunneling, inducing surface recombination and contributing to trap-assisted tunneling dark current.

The native oxides are readily generated on exposed device sidewalls saturating the dangling bonds and forming a secondary compound. Since thicknesses of InAs and GaSb SLS constituent layers are in order of tenths of MLs, whereas thicknesses of interfacial InSb and GaAs layers is commonly assumed to be less than a monolayer (ML) [30, 31], the formation of native oxides on GaSb and InAs is detrimental to the SLS device performance [32, 33].

Analysis of ternary phase diagrams [34] (Fig. 2) for gallium (indium)-based group III-group V-oxygen systems predicts the multilayered composition of the oxide film for the GaSb and InAs due to thermal oxidation with oxygen or water vapor in the air. The predicted oxide film composition is $GaSb/(Ga_2O_3 : Sb)/(Ga_2O_3 : Sb_2O_3)/GaSbO_4$ and $InAs/(In_2O_3 : As)/(In_2O_3 : As_2O_3)/InAsO_4$ for GaSb and InAs, respectively.

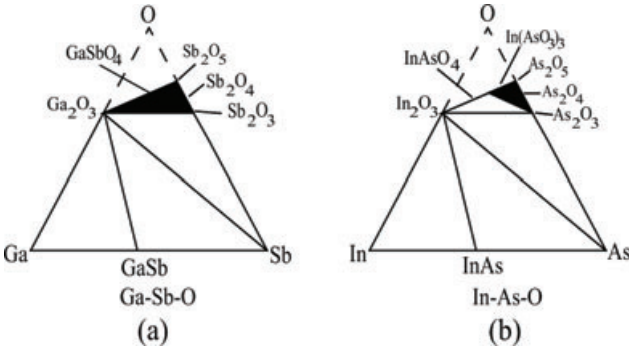

Figure 2 (a) Ga-Sb-O and (b) In-As-O equilibrium phase diagrams. Reprinted from [34].

The XPS studies carried out on oxidized GaSb [35] showed the presence of elemental Ga and Sb along with GaSb, Ga_2O_3, Sb_2O_3 and Sb_2O_5. XPS measurements [36] of oxidized InAs did not detect In_2O_3 and As_2O_3 phases as well as elemental As at the oxide-InAs interface. Instead, $InAs_xO_y$ oxide was detected at the interface with composition closer to $InAsO_3$ than to $InAsO_4$ and As was found to be distributed throughout the oxide film. The oxidation of GaSb and InAs may be summarized by the following stoichiometric reactions:

$$4GaSb + 3O_2 \longrightarrow 2Ga_2O_3 + 4Sb \quad (1)$$

$$In_2O_3 + As_2O_3 \longrightarrow InAsO_3 \quad (2)$$

Thus, the exposed to ambient atmosphere GaSb and InAs will react with atmospheric oxygen and form elemental antimony and indium oxide with elemental arsenic distributed through the oxide. The semi-metallic nature of elemental Sb results in the conduction channel parallel to the interface, which leads to increasing of surface component of dark current.

Unwanted native oxides need to be removed prior or during the pixel isolation process. The immersion in ammonium sulfide $[(NH_4)_2S]$ [33] immediately before the etch effectively removes native oxides with minimal surface etching due to the presence of $(NH_4)OH$ formed in water solution of $(NH_4)_2S$. Sample treatment with phosphoric acid based ($PO_4 : H_2O_2 : H_2O = 1 : 2 : 20$) or hydrochloric acid based ($HCl : H_2O = 1 : 10$) solutions will serve the same purpose [37]. Introduction of BCl_3 gas into the plasma chemistry is also effective in removal of native oxides and redeposited byproducts [38].

4. Single pixel isolation

Nowadays, high-density plasma etch processes are commonly utilized for InAs/GaSb SLS material in spite of inevitable degradation of sidewall surface electronic properties due to ion bombardment or unwanted deposition of etch by-products [39–42]. Plasma chemistry usually consists of chlorine-based precursors (BCl_3, Cl_2 or $SiCl_2$) due to high volatilities of gallium, indium, antimony and arsenide chlorides providing fast etch rates and smooth morphologies [43]. The resulting etch profiles are vertical due to the plasma sheath and the ionized gas directionality. Damage produced during the dry etch may be partially restored by subsequent chemical treatment [44]. Due to the ability of wet etches to cause virtually no surface electronic damage, a chemical etch attracts attention of researchers for single-pixel SLS device fabrication. However, the isotropic nature of wet etch process resulting in concave sidewall profile and an unavoidable tendency to undercut etch masks making precise dimensional control more difficult stipulates limited application of wet etches for SLS FPA fabrication.

Utilization of wet chemical etch process for fabrication of large area single pixel SLS detectors has been reported by various research groups (MWIR detectors [45–47] and LWIR detectors [47–49]). The choice of the appropriate wet chemical solution is complicated by dissimilar chemical properties of InAs and GaSb causing the preferential etch of either compound in SLS stack resulting in formation of ripples on the devices sidewalls, acting as an additional source for electrical active sites [50].

Chaghi et al. [45] compared different chemical solutions based on orthophosphoric (H_3PO_4) acid employed for fabrication of SLS detectors with cut-off wavelength of 4.9 µm at 80 K (3). Detector processed with $H_3PO_4/H_2O_2/H_2O/C_6H_8O_7$ (citric acid) followed by a second immersion in $NaClO : H_2O$ showed the best performance with R_0A of $1.6 \times 10^5\ \Omega\,cm^2$.

Kutty et al. [49] have reported on clean sidewalls profile with ~ 5 µm undercut obtained after hydrochloric (HCl)-based etch of 410 µm × 410 µm mesas of LWIR ($\lambda_{50\%} =$ 14 µm at 77 K) SLS detector. Das et al. [48] claimed the reduction of surface currents in LWIR ($\lambda_{50\%} = 8.8$ µm at 77 K) SLS detectors fabricated with combination of phosphoric and nitric based etchants.

320 × 256 LWIR ($\lambda_{100\%} = 10$ µm at 77 K) FPA with 30 µm pitch fabricated by wet etch technique was demon-

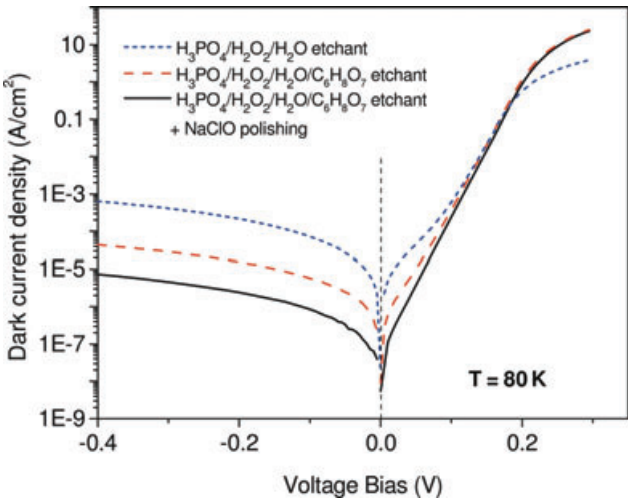

Figure 3 (online color at: www.lpr-journal.org) Dark current density measured at 80 K for MWIR ($\lambda_{50\%} = 4.9\,\mu m$ at 80 K) InAs/GaSb SLS photodiodes with mesa size of 465 µm fabricated with different etch schemes. Reprinted from [45].

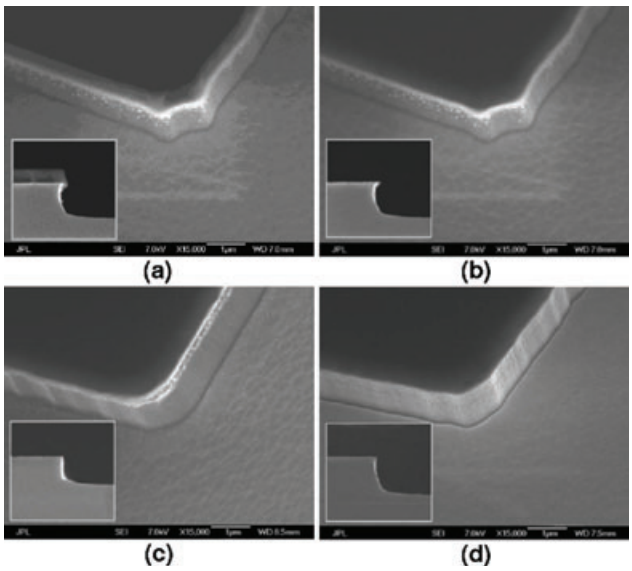

Figure 4 SEM pictures of the four different etched samples. The inset in each SEM picture provides the corresponding cross-section profile. Sidewall angles were measured to be 54.9° (sample A), 72.8° (sample B), 87.9° (sample C), and 81.1° (sample D). Reprinted from [52].

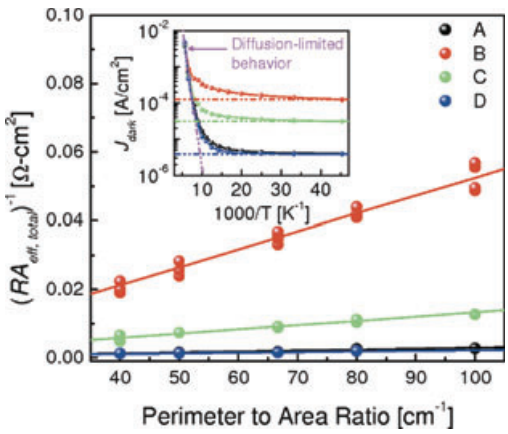

Figure 5 (online color at: www.lpr-journal.org) RA_{eff} at $T = 77$ K and 0.2 V bias for different sized diodes. The inset is a plot of dark current density as a function of detector temperature. Reprinted from [52].

strated by QmagiQ [51], with dark current density of to 2×10^{-4} A/cm^2 (77 K) at 0.3 V bias. Despite the relatively high dark current density the NEDT had acceptably low values mainly due to the high quantum efficiency (45% at 0.3 V), a key finding for SLS FPA viability.

Inductively coupled plasma (ICP) etch with chlorine-based chemistry was employed by Ngyuen et al. [52] for pixel isolation of SLS LWIR ($\lambda_{50\%} = 10.3\,\mu m$ at 77 K) detectors. Four samples with different etch conditions were studied: a $C_4H_6O_6 : H_3PO_4 : H_2O_2 : H_2O$ wet etch followed by a citric clean-up dip (sample A); a BCl_3-Ar dry etch followed by a citric clean-up dip (sample B); a CH_4-H_2-Ar plasma (sample C); and a BCl_3 -Cl_2-CH_4-H_2-Ar plasma (sample D). Figure 4 presents SEM pictures of 200 µm × 200 µm detectors showing both the sidewall morphology and cross-section profile for all the etch schemes. Vertical ripples on the sidewalls, and also a significant amount of undercut with sidewalls sloped at an angle of 54.9° was observed for sample A. The preferential etching in samples B and C has resulted in "waffle"-like pattern observed in the plane of the mesa. In addition, the indium droplets on the sidewalls of sample B were due to the low volatility of $InCl_x$. This effect may be compromised by using higher etch temperatures and increased ion energy values, however, it would result in increased amount of sputtering and more pronounced preferential etching. Sample D exhibited smooth sidewalls with no preferential etching, inferred from the lack of the waffle-like pattern, or indium residuals.

The amount of surface leakage provided by each investigated etch scheme was characterized by the size-dependent effective resistance-area product, RA_{eff}, as shown in Fig. 5. Samples A (wet etch) and D (BCl_3-Cl_2-CH_4-H_2-Ar plasma etch) showed relatively flat behavior compared to the other samples, with a surface resistivity that is at least 7.4 times higher. Combination of chlorine- and methane-based etches resulted in electrical device performance comparable to the wet etched samples, moreover, near-vertical, smooth sidewalls with minimal dielectric mask erosion were achieved with good anisotropy resulting in more than three times higher fill factor.

The electron cyclotron resonance (ECR)-reactive ion etching is alternative high density plasma approach of InAs/GaSb SLS mesa definition. Huang et al. [42] compared electrical performance of LWIR ($\lambda_{50\%} = 9.3\,\mu m$ at 77 K) InAs/GaSb SLS detectors fabricated with ICP and ECR etching techniques. Both processes were based on BCl_3 : Ar chemistry, for protection of etched sidewalls SiO_2 and polyimide were utilized separately. The ECR process

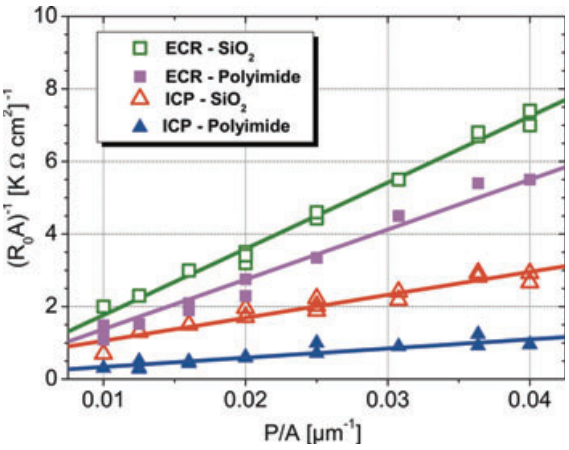

Figure 6 (online color at: www.lpr-journal.org) The $1/R_0A$ as a function of P/A for diodes between 100 and 400 μm in diameter at 77 K. Reprinted from [42].

was followed by citric acid-based wet etch to remove plasma induced surface damage. Figure 6 shows the inverse R_0A product vs P/A for detectors with mesa sizes ranging within 100–400 μm. Detector etched by ICP with sidewalls encapsulated by polyimide has demonstrated the highest surface resistivity ($6.7 \times 10^4\ \Omega \cdot$ cm) among four treatments. Comparison of electrical performance of detectors etched with ECR and ICP with the same post-etch encapsulation method (polyimide) revealed an order of magnitude lower dark current density for ICP-polyimide sample. This is attributed to the better surface conditions prior passivation achieving by ICP.

In conclusion, plasma assisted etch with combination of BCl_3, CH_4, and Ar gases seems to be the optimal approach for the edge definition of InAs/GaSb SLS detectors providing nearly vertical profiles and clean sidewalls free from etch residues.

5. Passivation of InAs/GaSb SLS detectors

An ideal passivant must satisfy the following criteria:

1. Prevent chemical reactions between ambient atmosphere and the semiconductor surface (chemical passivation);
2. Eliminate and prevent the formation of interface states in the band gap of semiconductor (electrical passivation);
3. Serve as an energy barrier for charge carriers at the interface, i.e. possess a sufficient energy barrier such that electrons will not be lost from the semiconductor surface to the passivating layer;
4. Exhibit thermal and long term stability. In other words, passivation layer must not undergo any change in its constitutional, physical and interfacial properties at variable temperatures (10–300 K) during the lifetime of the SLS detector (typically, 10,000 hrs);

Work on passivation of bulk III-V semiconductor surfaces was following in two main directions, as stated in [53]. The first one is deposition of relatively thick insulator layers. In this case, the semiconductor/insulator heterojunction with properties defined by the density of states at the interface is formed. The second direction is modification of the atomic structure of the surface by foreign atoms which changes the electronic structure of the semiconductor surface. Our paper employs the same categorization of passivation methods of InAs/GaSb SLS detectors, in particular, encapsulation of etched sidewalls with thick layers of dielectrics, organic materials (polyimide and various photoresists), or wider-band gap III-V material, and chalcogenide passivation, that is saturation of unsatisfied bonds on semiconductor surface by S-atoms.

The effectiveness of passivation is commonly evaluated using variable area diode array (VADA) method [54]. For the square mesa diode, the dark current density can be expressed as the summation of bulk component of dark current and the surface leakage current. If the bulk current dominates the detector performance, then the curve will have a slope close to zero. If the surface leakage is significant, then an increase in the dark current density will be observed for smaller devices. In other words, the surface dependence of inverse of the dynamic resistance-area product at zero bias R_0A of passivated diode can be approximated as

$$\frac{1}{R_0A} = \frac{1}{R_0A_{\text{Bulk}}} + \frac{1}{r_{\text{Surface}}}\frac{P}{A} \tag{3}$$

where $(R_0A)_{\text{Bulk}}$ is the bulk R_0A contribution ($\Omega\,\text{cm}^2$), r_{Surface} is the surface resistivity ($\Omega\,\text{cm}$), P is the diodes perimeter and A is the diodes area. The slope of the function given by equation (3) is directly proportional to the surface-dependent leakage current of the diode. Higher values of surface resistivity indicate weaker dependence of the diode's characteristics on the surface effects. Figure 7 schematically illustrates the $(\frac{1}{R_0A})$ vs $(\frac{P}{A})$ dependence for the diode with ideal and non-ideal passivations.

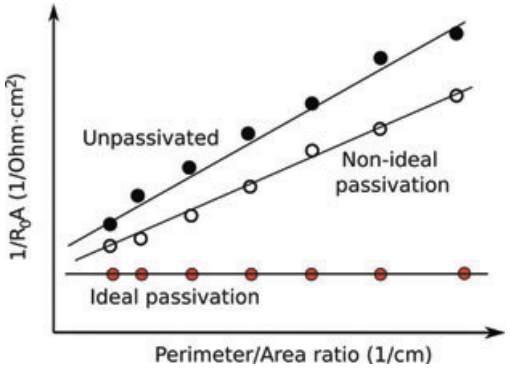

Figure 7 (online color at: www.lpr-journal.org) Dependence of the dynamic resistance-area product at zero bias vs. perimeter-to-area ratio for VADA diodes with ideal and non-ideal passivations.

5.1. Dielectric passivation

Gin et al. [38] reported passivation of InAs/GaSb SLS detectors with SiO_2 resulted in improvement of zero-bias resistance by a factor of 2, which leads to a detectivity improvement of 41%, assuming all other variables remain the same

as with unpassivated detectors. The best passivation results were achieved with SiO_2 grown in plasma enhanced chemical vapor deposition (PECVD) system at 160°. It should be noted that the typical temperature of SiO_2 deposition in a PECVD system is 320° [55]. Special care has to be taken to develop a low-temperature process of high-quality SiO_2 deposition to prevent SLS period intermixing.

Hood et al. [14] utilized SiO_2 for passivation of very-long wavelength ($\lambda_{50\%\ \text{cut-off}} = 12.0\,\mu\text{m}$ at 77 K) IR InAs/GaSb SLS detectors. Approximately 300 nm of silicon dioxide was deposited by PECVD at a susceptor temperature of 160°. The R_0A fell in the 0.02–0.07 $\Omega\,\text{cm}^2$ range for nearly all passivated diodes. Figure 8 presents the dependence of $(R_0A)^{-1}$ on the perimeter-to-area ratio for passivated and unpassivated diodes. A surface resistivity was evaluated to 7 Ω cm and 33 Ω cm for unpassivated and silicon dioxide passivated devices, respectively.

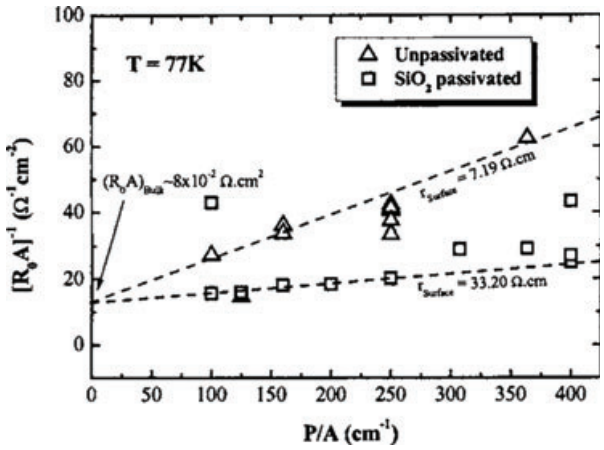

Figure 8 Dependence of (R_0A^{-1}) on the perimeter-to-area ratio for passivated and unpassivated diodes for InAs/GaSb SLS VLWIR detectors. Reprinted from [14].

Nolde et al. [56] have investigated relationship between thickness and composition of native oxides on LWIR ($\lambda_{50\%\ \text{cut-off}} = 8.75\,\mu\text{m}$ at 77 K) InAs/GaSb SLS detector sidewalls prior SiO_2 deposition and diode performance. The best surface resistivity ($4.38 \times 10^6\ \Omega\,\text{cm}$) was demonstrated by detector with ozone-enhanced native oxides.

The method to control band-bending at SLS-SiO_2 interface has been recently proposed by Chen et al. [57]. By applying a negative bias voltage along MWIR ($\lambda_{50\%\ \text{cut-off}} = 4.7\,\mu\text{m}$ at 110 K) SLS devices sidewall the accumulated electrons repel from the insulator/SLS interface thus establishing flat-band conditions which suppress the leakage current. The schematic diagram of gated diode MWIR type-II SLS based on p-p-M-n heterojunction [58] and comparison of electrical performance at low temperatures for gated and ungated diodes is shown in Figs. 9 and 10, respectively.

Dielectric passivation, though shown to be effective, presents the challenges of developing high-quality, low fixed and interfacial charges density dielectrics at process temperatures substantially lower that the InAs/GaSb SLS growth temperature to prevent the SLS period intermixing. Moreover, dielectric passivation layer alters the band bending presented at mesa sidewalls caused by abrupt termination of the periodic crystal structure. This band bending induces accumulation or type inversion of charge resulting in surface tunneling currents along sidewalls. As was shown by Delaunay et al. [59], the narrow bandgap devices (with bandgap of 120 eV or lower) are more susceptible to the formation of charge conduction channels along the sidewalls. Native fixed charges presented in dielectric passivation layer (e.g. SiO_2) can either improve or deteriorate the device performance [57], consequently, the dielectric passivation may not passivate the low band gap materials as effectively as high bandgap materials. Despite all of the potential drawbacks, the dielectric (SiO_2) passivation attracts attention of researches for passivation of LWIR SLS detectors because it is compatible with current FPA fabrication procedures

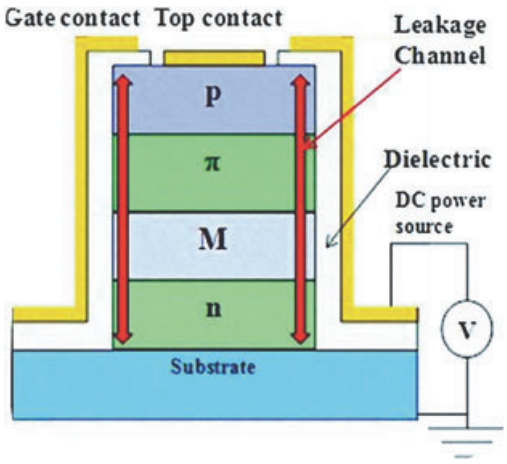

Figure 9 (online color at: www.lpr-journal.org) Schematic diagram of gated diode. Reproduced from [57].

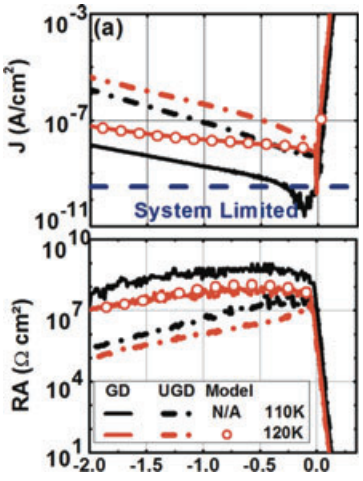

Figure 10 (online color at: www.lpr-journal.org) Current-voltage and resistance-voltage measurements of ungated (UGD, dot-dash) and gated (GD, solid-line) diodes at 110 K and 120 K. Reproduced from [57].

5.2. Passivation with organic materials

Organic materials (polyimide or various photoresists) are attractive for the passivation of InAs/GaSb SLS detectors

due to simple integration into fabrication procedure. Usually they are spin-coated at room temperature with different speeds that give rise to film thicknesses in the range of 0.2–100 μm.

Passivation of MWIR [60, 61] and LWIR [62] SLS detectors with SU-8 has been reported. SU-8 is a high-contrast epoxy-based negative photoresist, which was developed by IBM [63]. Presently, SU-8 is widely used in MEMs [64] and optoelectronics applications [65]. SU-8 consists of a bisphenol A novolak epoxy resin, a photo initiator, and solvent γ-butyroalectone [66]. The photo initiator is easily broken down and changes into strong acid ($HCbF_6$) upon exposure of UV. This acid causes a high cross-link density in the SU-8 film, thereby leading to an increase in its chemical resistance to the developer. Photo-polymerized SU-8 is mechanically and chemically stable after a hard bake.

Comparison of unpassivated and SU-8 passivated single pixel SLS MWIR devices ($\lambda_{50\%\ \text{cut-off}} = 4.6\,\mu\text{m}$ at 77 K [60]) resulted in four orders of magnitude reduction in dark current density (from 8×10^{-3} to 5×10^{-7} A/cm^2 at an applied bias of -0.3 V), and fivefold increase in the surface resistivity (from 1.9×10^{2} to $1.0\times10^{3}\ \Omega\cdot$cm at 87 K). DeCuir et al. [61] investigated the effect of SU-8 passivation on MWIR ($\lambda_{50\%\ \text{cut-off}} = 4.9\,\mu\text{m}$ at 77 K) SLS detectors preceded by the nonaqueous thioacetamide treatment or ammonium sulfide treatment. Figure 11 presents inverse R_0A vs. P/A of diodes for two sets of variable area diodes (ranging from 40–400 μm) using either ammonium sulfide or thioacetamide pre-treatment. The eight-fold increase in surface resistivity of SU-8 passivated diodes pre-treated with nonaqueous thioacetamide has been observed as compared with aqueous ammonium sulfide.

Passivation of LWIR ($\lambda_{100\%\ \text{cut-off}} = 12\,\mu\text{m}$ at 77 K [62]) InAs/GaSb SLS detector resulted in a 30-fold reduction in the dark current density at a low value of applied bias ($V_b = -0.1$ V) for the small area (50 μm × 50 μm) devices,

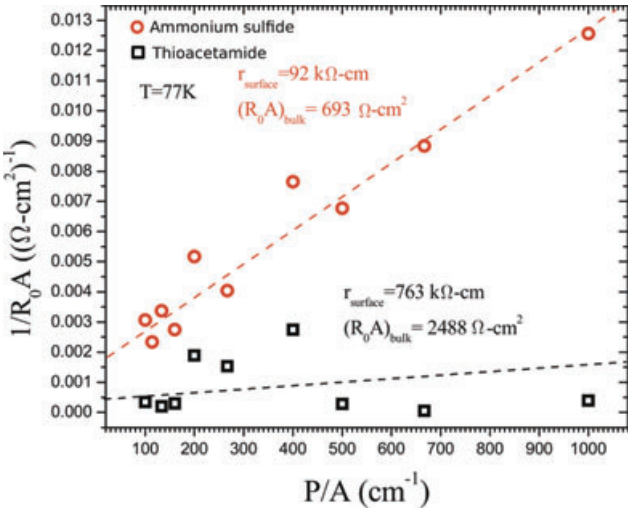

Figure 11 (online color at: www.lpr-journal.org) inverse R_0A vs. P/A of diodes for two sets of variable area diodes (ranging from 40–400 μm) using either ammonium sulfide or thioacetamide pre-treatment. Reprinted from [61].

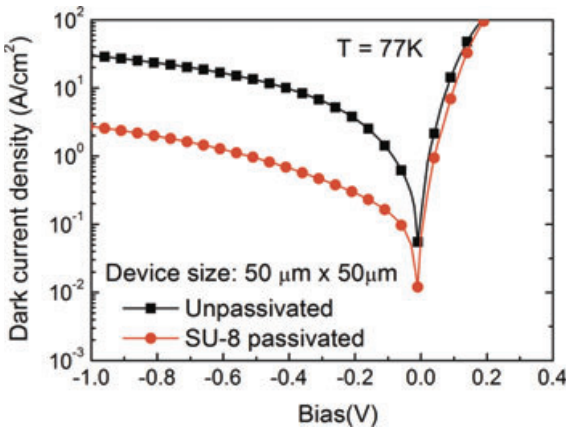

Figure 12 (online color at: www.lpr-journal.org) Dark current density vs applied bias for LWIR unpassivated and SU-8 passivated small area device. Reprinted from [62].

as shown in Fig. 12. It should be noted that a considerable degree of nonuniformity of dark current densities for unpassivated devices was observed and the uniformity was improved after the SU-8 passivation.

Hood et al. [67] reported on passivation of InAs/GaSb LWIR SLS detectors ($\lambda_{100\%\ \text{cut-off}} = 11.0\,\mu\text{m}$ at 77 K) with polyimide layer. Polyimides (sometimes abbreviated PIs) are polymers of imide monomers, widely known for their thermal stability, good chemical resistance, and excellent mechanical properties. In performed study, conformal polyimide (PI-2555, HD Microsystems) was spun onto the sample with defined mesas. Imidization was carried with gradual ramping of the temperature to 180° and curing for ∼ 45 min. Figure 13 illustrates the I-V curve from polyimide passivated device with side ranging in size from 25 to 50 μm. Inset in Fig. 13 shows the zero-bias inverse dynam-

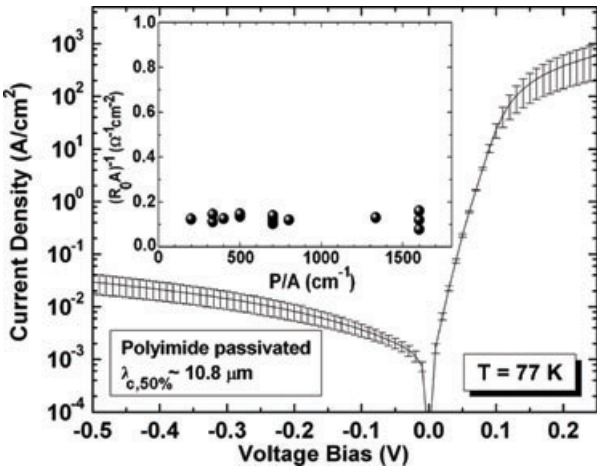

Figure 13 The I-V curves from polyimide passivated devices with side ranging in size from 25 to 50 μm. Solid lines represent an average IVs, whereas standard deviation is presented by vertical bars. Inset shows the zero-bias inverse dynamical impedance R_0A^{-1} vs perimeter-to-area ratio for the various sizes of passivated devices. Reprinted from [67].

ical impedance $(R_0A)^{-1}$ vs perimeter-to-area ratio for the various sizes of passivated devices. No surface dependence was observed and diodes R_0A values were found within the range of ~ 6–$13\,\Omega\,\mathrm{cm}^2$. Moreover, authors found that prolonged vacuum desorption (288 hrs) performed prior polyimide passivation helped to improve the uniformity of R_0A values and to bring the zero-bias electrical behavior close to the near bulk-limited case. In addition, polyimide passivation was shown to be stable upon exposure to various ambient conditions as well as over time. The polyimide passivated devices (LWIR,$\lambda_{100\%\ \text{cut-off}} = 10.0\,\mu\mathrm{m}$ at 77 K) were measured again after 3 months of storage in ambient conditions [44]. The same R_0A and perimeter/area trend as in the initial measurement were obtained, which confirmed the long-term stability of this passivation technique.

Chaghi et al. [45] reported on passivation of the MWIR InAs/GaSb SLS detector ($\lambda_{50\%\ \text{cut-off}} = 4.9\,\mu\mathrm{m}$ at 80 K) sidewalls with photoresist. Photoresist AZ-1518 was spun onto the sample right after the mesa etching and heated at 200°C for 2 hr to be polymerized. It was found that photoresist effectively protects the device sidewalls from oxidation in ambient atmosphere, moreover, performance of passivated devices was not degraded over three weeks suggesting good long-term stability of photoresist passivation.

5.3. Passivation with wide-bandgap materials

Surface currents may be suppressed by reduced exposure of narrow gap materials to the environment, e.g. as a result of encapsulation of etched sidewalls with wide band gap material or "shallow etch" technique that isolates the neighboring devices but terminates within a wider bandgap layer.

Rehm et al. [43] have suggested passivation of SLS InAs/(In,Ga)Sb LWIR photodiodes ($\lambda_{50\%} = 10\,\mu\mathrm{m}$ at 77 K) by subsequent overgrowth of lattice matched, large-bandgap semiconductor layer ($Al_xGa_{1-x}As_ySb_{1-y}$) over etched mesa sidewalls. The cross-section of completely processed InAs/(In,Ga)Sb SLS photodiode passivated by MBE overgrowth with AlGaAsSb is shown in Fig. 14. Position of the Fermi level at the interface can be adjusted by variation of doping concentration of the large-gap semiconductor material. In order to prevent Al-containing passivation layer from oxidation, thin (200 nm) layer of silicon nitride was deposited after re-growth process.

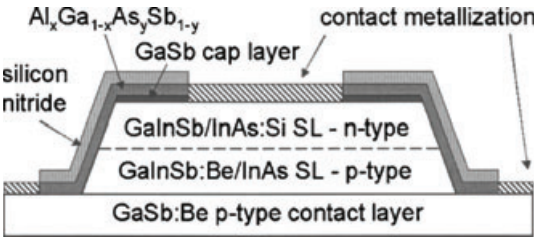

Figure 14 The cross-section of completely processed InAs/(In,Ga)Sb LWIR SLS photodiode passivated by MBE overgrowth with AlGaAsSb. Reprinted from [43].

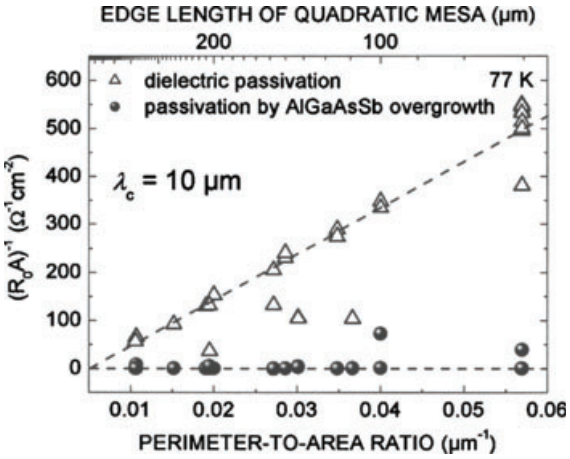

Figure 15 Dependence of R_0A^{-1} vs perimeter-to-area ratio for the two similar detector structures, passivated by the overgrowth and by the conventional dielectric layer passivation. While the dielectric passivation leads to a strong degradation by surface leakage currents, no surface leakage is observed for overgrowth passivation. Reprinted from [43].

Figure 15 illustrates the dependence of (R_0A) vs perimeter-to-area ratio for the two similar detector structures, passivated by the overgrowth and by the conventional dielectric layer passivation. The overgrowth technique reduces surface leakage currents by three orders of magnitude reaching the bulk R_0A value of InAs/(In,Ga)Sb SLS photodiode.

Mesa sidewalls encapsulation with GaSb to eliminate the surface currents in InAs/GaSb FPAs has been proposed by Szmulowicz and Brown [68]. In an offered scheme, the GaSb encapsulant acts a barrier to electrons at both the n- and p-sides of the SLS and as a well for the minority holes on n-side of the junction. Thus electrons are confined in the SLS whereas holes are depleted from the active volume of the device. The surface currents are reduced by eliminating sidewalls, in addition, the SRH and Auger recombination lifetimes are expected to be higher due to reduction of hole density in the depletion region.

Aifer et al. [69] proposed the shallow-etch mesa isolation (SEMI) approach for the device definition. The neighboring photodiodes are isolated from one another by etching just deep enough to break the doping-defined junction and to leave the narrower-gap IR-absorbing layer buried below of wider-gap material. SEMI restricts the exposed surfaces to the wide-band gap layers, thus suppressing the surface recombination and the ability of surface electric fields to produce conducting channels that would bypass the junction. Figure 16 shows the comparison of dark current densities of LWIR ($\lambda_{50\%} = 10.2\,\mu\mathrm{m}$ at 77 K) SLS detectors processed with deep and SEMI etches and fits of inverse $R_{\mathrm{eff}}A$ versus perimeter-to-area ratio for the same devices.

Passivation of narrow bandgap SLS material with wide bandgap materials regrown on sidewalls of fabricated device by MBE is an effective technique for the surface leakage current reduction. However, this passivation approach requires very careful surface cleaning prior the overgrowth proce-

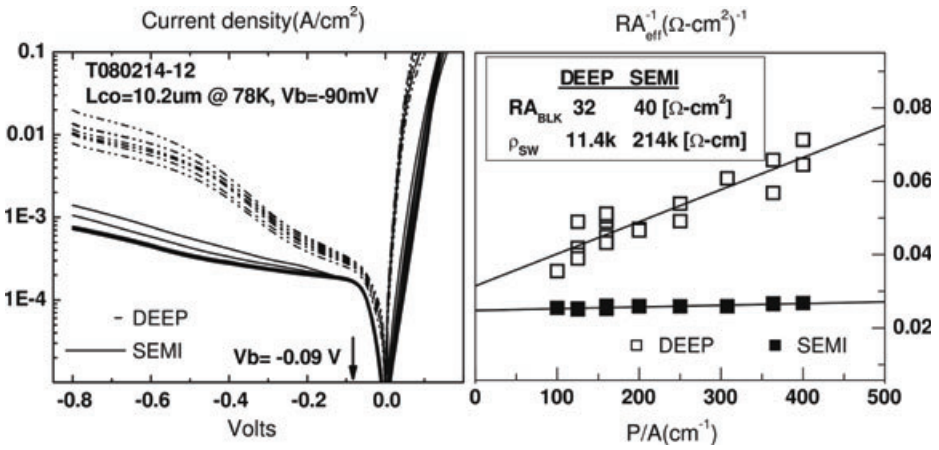

Figure 16 Comparison of dark current densities of LWIR ($\lambda_{50\%} =$ 10.2 µm at 77 K) SLS detectors processed with deep and SEMI etches (left). Fits of inverse $R_{\text{eff}}A$ versus perimeter-to-area ratio for the same devices (right). Reprinted from [69].

dure, which significantly complicates the integration of this passivation methods into fabrication process of detectors and FPAs.

The "buried" architecture of InAs/GaSb SLS detectors realized with "shallow etch" technique excludes the need for the passivation. Due to the way detectors are fabricated, the size of the device is not defined by the etch dimensions but by the lateral diffusion length of minority carriers. If the values of lateral diffusion length are larger than the distance between neighboring pixels in the FPA, crosstalk between the FPA elements can be encountered. Presence of crosstalk in the FPA could lead to degradation of image resolution. Although Aifer et al. [69] did not observe the evidence of cross-talk for 256 × 256 FPA with 40 µm pitch and 24-µm-wide SEMI mesas based on graded bandgap W-structure, the further investigation of SEMI approach realized on SLS detectors based on different heterostructures is needed.

5.4. Chalcogenide passivation

Other approach for passivation of InAs/GaSb SLS detectors is chalcogenide passivation. In the past there were a number of reports on the improved electronic properties of chalcogenide-passivated III-V materials. In particular, enhanced photoluminescence (PL) and band bending were observed on passivated GaAs (001) surfaces [70–72]. Based on the photoreflectance measurements, Paget et al. [73] proposed that the formation of Ga-S bond was responsible for the reduction of surface states within the forbidden gap.

Passivation of InAs (001) surface by ammonium sulfide solution was also studied [74, 75]. It was found that passivation effectively removes native oxide with the minimal surface etching and creates a covalently bonded sulfur layer. Final structure of passivated InAs surface can be represented by S-on-In-on-As "layer-cake" model.

In order to improve the GaSb surface characteristics, various surface passivation processes have been studied based on wet or dry chemical processing. Stimulated by the successful application of sulfide passivation of GaAs surfaces, the passivation of GaSb surfaces by alkaline sulfides, including Na_2S and $(NH_4)_2S$ in aqueous solutions, have been studied by several research groups [76–78]. Observation of enhanced PL intensity and reduced diode leakage current indicated the improvement in the electrical and optical properties of the GaSb surface by sulfur-based treatments.

The theory of chalcogenide passivation is developed for the most studied material among III-V compounds, GaAs [72, 79, 80]. The reduction in the density of surface states by chalcogenide passivation was attributed to the formation of an ordered layer of sulfur adatoms on the surface. Electronic structure of the passivated surface could be predicted theoretically based on the suitable choice of reconstruction, optimization of the position of the atoms on the surface due to total energy minimization, and calculation of the density of electronic stated distribution for the given atomic structure. Follow this procedure, Ohno et al. [81, 82] reported the theoretical calculation results for ideal GaAs (001)-1 × 1 surfaces with a full monolayer of S atoms adsorbed on either the Ga- or As- terminated surface. They found that surface bridge sites were energetically favorable for S adsorption.

The interactions between the Ga dangling bond and the S sp^3 orbitals form the bonding and anti-bonding states. The fully filled bonding states are located within the valence band, while the empty anti-bonding states are in the conduction band. Therefore the S adsorption on an ideal Ga-terminated surface replaces the mid-gap Ga-related surface states with a low-lying S-induced surface states. However, on an As-terminated surface, the S-As anti-bonding states are still within the energy gap and they are partially filled with electrons, preventing the reduction of the gap-region surface state density.

In general, mechanism of formation of passivation coating for III-V compound can be divided into two stages:

1. Removal of oxide layer from the surface
2. Transfer of electrons from the semiconductor into the solution and formation of chemical bonds between semiconductor and sulfur atoms

Bessolov and Lebedev [53] described the sulfidization of III-V semiconductors from solutions of inorganic sulfides as an red-ox reaction

$$\mathrm{A^{III}B^{V} + HS^{-} + R - OH} \longrightarrow (\mathrm{A^{III}})_{x'}\mathrm{S}_{y'} + (\mathrm{B^{V}})_{x''}\mathrm{S}_{y'} + \mathrm{R - O^{-} + H_2} \qquad (4)$$

here R is a hydrogen atom (for aqueous solutions) or an alkyl group (for alcohol solutions). The sulfide coating is a mixture of different sulfides, since the stoichiometric coefficients x' (x'') and y' (y'') can vary from 1 to 5.

It was proposed the formation rate of sulfur passivating coating should increase with increasing treatment temperature, the concentration of sulfur atoms in the solution and with reduction of pH of the solution.

From the passivation study of GaAs it was found the sulfidization of III-V semi- conductors proceeds more efficiently in alcohols than in water. It was attributed to the lower dielectric constants of alcohols: a less polar medium allows a stronger electrostatic interaction between solution ions and the semiconductor surface. Liu et al. [83–85] investigated non-aqueous versus aqueous-based passivation of GaSb (100) surfaces. A non-aqueous passivation solution contained a sodium sulfide in anhydrous benzene. To increase solubility of sodium sulfide, a cation complexing agent, 15-crown-5, was added to the solution. Aqueous passivation consisted of the immersion of GaSb wafers in saturated Na_2S aqueous solution. The aqueous passivation resulted in a threefold increase in PL intensity whereas non aqueous passivation resulted in marked enhancement in PL intensity. In addition, the non-aqueous passivation process exhibited higher sulfide coverage, lower content of the residual oxide as well as elemental Sb.

5.4.1. Ammonium sulfide passivation of InAs/GaSb SLS detectors

Passivation of InAs/GaSb SLS detectors with aqueous ammonium sulfide solutions is easily integrated into fabrication sequence, since it is performed simply by immersion of sample in $(NH_4)_2S$-based solutions. Moreover, no native oxide removal step is required prior passivation, since the native oxides are etched by $(NH_4)OH$ formed in water solution of ammonium sulfide.

Gin et al. [86] reported passivation of InAs/GaSb LWIR ($\lambda_{100\%\ \text{cut-off}} = 8\,\mu m$ at 77 K) SLS detectors with various solutions of ammonium sulfide. The soaking of 400 µm × 400 µm square mesa samples in full-strength ammonium sulfide [$(NH_4)_2S$ 20%] solutions for 15 minutes resulted in reduction of dark current density by factor of 2 and improvement of maximal differential resistance by factor of 3 compared with unpassivated devices. However, examination of the passivated samples under the scanning electron microscope revealed the severe undercut of the detector mesas and etching of the GaSb buffer layer. To reduce the deleterious effect of dull-strength ammonium sulfide solution, samples were treated with the $(NH_4)_2S$ solution diluted in four parts of de-ionized water for the same time. No visible damage on sidewalls was observed, and dark current density was reduced at least by two orders of magnitude as compared to unpassivated samples (Fig. 17). With increased time of passivation treatment the efficiency of passivation was improved. The average values of differential resistance were 18.23 kΩand 19.61 kΩfor 15 and 30 min passivation, respectively, versus 970 Ωfor the unpassivated detectors.

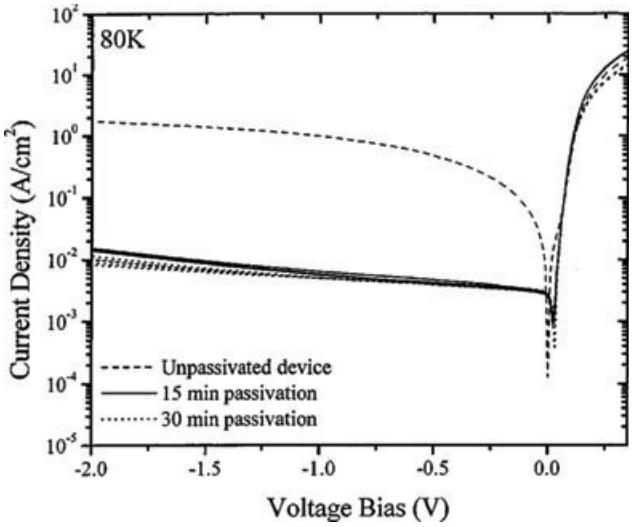

Figure 17 Dark current density vs voltage bias for unpassivated and $(NH_4)_2S$:H_2O passivated detectors at 80 K. Reprinted from [86].

Plis et al. [37] used the diluted solution of ammonium sulfide for passivation of InAs/GaSb LWIR SLS detectors ($\lambda_{100\%\ \text{cut-off}} = 12\,\mu m$ at 77 K). Samples were immersed in passivation solution for two hours. The dark current density of 50 µm × 50 µm devices was reduced by factor of 25 compared to unpassivated devices.

The mechanism of ammonium sulfide passivation on LWIR InAs/GaSb SLS detectors was in details investigated by Banerjee et al. [33]. X-ray photoelectron spectroscopy (XPS) measurements were performed on as-etched with phosphoric acid based solution ($H_3PO_4 : H_2O_2 : DIH_2O = 2 : 1 : 20$ for 1 min) and ammonium sulfide treated (24% aqueous $(NH_4)_2S$ solution at 60° for 15 min) LWIR SLS samples. Figure 18 shows XPS spectra obtained for as-etched and $(NH_4)_2S$-treated samples for In (Fig. 18a), As (Fig. 18b), Ga (Fig. 18c), and Sb (Fig. 18d).

The sulfur peak in the range of 161 eV to 165 eV [87] corresponding to the binding energy of sulfur $2p_{3/2}$ bonded to In, As, Ga, or Sb was too weak on either sample and could not be distinguished from the background. The results indicate that no sulfur bonds were created during the treatment. However, it is also clear that the oxides were removed effectively and the surface was sustained after 30 min of exposure to air, indicating weak sulfidization. The XPS measurements were repeated on the same samples exposed to the ambient atmosphere for ten days and revealed reappearance of the detrimental oxides on the surface of treated samples earlier also observed by other researchers [88].

In conclusion, the aqueous ammonium-sulfide treatment showed the short-term benefits for performance of InAs/GaSb SLS LWIR detectors. However, the treatment may cause the degradation of device performance attributed to the secondary oxidation, since the hydrophobic surface generated by oxide removal step repels the solution and

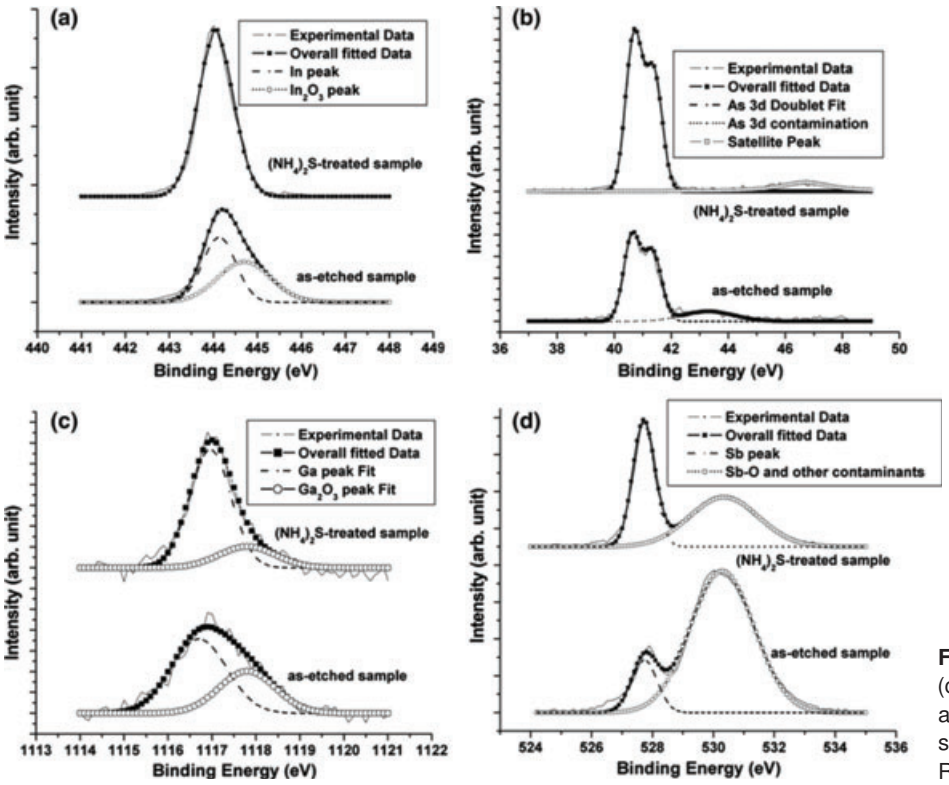

Figure 18 (a) In $3d_{5/2}$, (b) As 3d, (c) Ga $2p_{3/2}$, and (d) Sb $3d_{5/2}$ of as-etched (bottom) and ammonium sulfide treated (top) SLS samples. Reprinted from [33].

leaves the surface exposed for O_2-re-adsorption. In addition, temporal instability of such passivation layer was observed and the necessity for a suitable capping layer to preserve good passivation quality in the long term was reaffirmed.

5.4.2. Thioacetamide passivation

Thioacetamide (C_2H_5NS or TAM) has been proposed as an alternate sulfidizing agent for the passivation of GaSb and InAs surfaces [89] as well as GaInAsSb [90] and InAs/GaSb LWIR [91] photodiodes. Depending on preparation the TAM solution may be acidic or basic, in contrast with always basic aqueous solution of $(NH_4)_2S$. As a result, TAM treatment offers formation of more stable M-S bonds, where M is Ga, In, As or Sb, than ammonium sulfide treatment resulting in weaker M-O-S bonds. Moreover, the TAM treatment does not produce elemental antimony on the semiconductor surface.

The acidic TAM passivation of LWIR InAs/GaSb SLS mesa-etched photodiodes resulted in four times improvement of R_0A value ($590\,\Omega\,cm^2$ at 85 K) compared to ammonium sulfide treated diodes. However, the XPS studies revealed the reappearance of surface oxides on the TAM treated surface after long term air exposure asserting the need for a suitable capping layer.

5.4.3. Electrochemical passivation of InAs/GaSb SLS detectors

Electrochemical passivation (ECP) of MWIR ($\lambda_{100\%\ \text{cut-off}} = 4.5\,\mu m$ at 77 K) and LWIR ($\lambda_{100\%\ \text{cut-off}} = 10\,\mu m$ at 77 K) InAs/GaSb SLS photodiodes has been demonstrated by Plis et al. [92]. The ECP cell consisted of the sample (anode), a platinum mesh electrode (cathode) and the electrolyte (0.1 M Na_2S in ethylene glycol) in a glass beaker at room temperature. The deposited sulfur-rich layer was ~ 50 Å thick and uniformly distributed over exposed sidewalls.

Figure 19 shows three orders of magnitude improvement in R_0A product for MWIR SLS detector at 50 K after ECP. To measure the stability of the passivation, dark current densities were measured for the as-processed and passivated

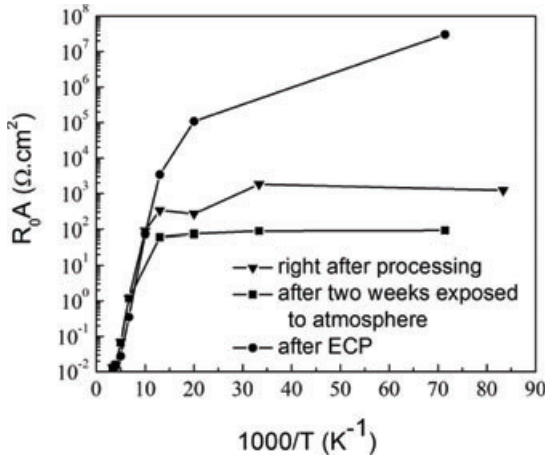

Figure 19 Dynamic impedance-area product at zero bias R_0A against temperature measured for as-processed, stored two weeks without inert atmosphere and passivated MWIR SLS detectors. Reprinted from [92].

devices. No considerable degradation of dark current density for passivated device was observed even after 12 weeks after ECP.

ECP of LWIR InAs/GaSb SLS detectors (mesa area of 50 µm × 50 µm) resulted in dark current reduction by two orders of magnitude, as shown in Fig. 20. Surface resistivity $r_{surface}$ was equal to 6 and 2717 Ω cm^2 for the unpassivated and ECP treated detectors, respectively.

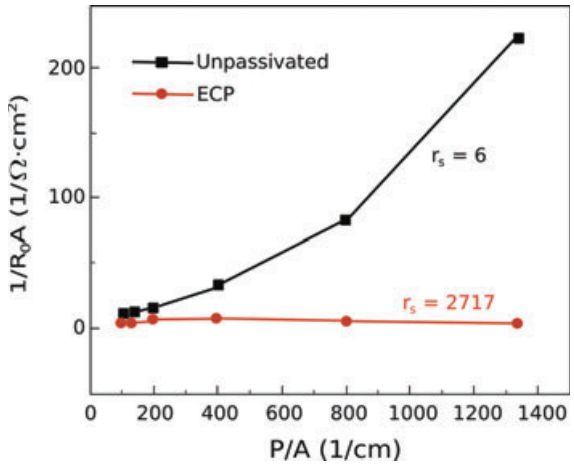

Figure 20 (online color at: www.lpr-journal.org) Dependence of dynamic resistance-area product at zero bias vs (P/A) ratio for unpassivated and ECP passivated LWIR SLS diodes with variable areas at 77 K. Reproduced from [37].

The long-term stability of ECP treatment was evaluated by measuring I-V characteristics of the LWIR SLS detectors treated with ECP right after the passivation and four weeks later [37]. The detector performance did not degrade for the large area device (400 µm × 400 µm), whereas the dark current density increased by a factor of ∼ 5 for the smallest area device (30 µm × 30 µm). This is attributed to the reaction of sulfur with oxygen in the air to form SO_2 gas. Thus, the encapsulation with some type of dielectric material (e.g. SiN_x, SiO_2 or SU-8) is required to prevent the ECP passivation from degradation.

In summary, ECP treatment is effective for the dark current reduction in MWIR and LIWR InAs/GaSb SLS detectors. However, thin (50 Å) sulphur layer deposited through ECP may oxidize easily and additional encapsulation is required.

5.4.4. ZnS passivation of InAs/GaSb SLS detectors

ZnS is an attractive candidate for the passivation of InAs/GaSb SLS detectors, since it effectively saturates the dangling bonds with sulfur and acts as self-encapsulant, preventing desorption of sulfur atoms from the surface. Moreover, electron-beam evaporated ZnS showed relatively small fixed charge density [93] with which the SLS detector sidewalls surface is hardly inverted or accumulated to induce tunneling current. Typical thickness of ZnS film is 200–400 nm, the deposition rates are 0.6–0.7 Å/s below 500 Å and 1–1.2 Å/s until the end. A slower initial deposition rate is maintained to help the passivant molecule to find the minimum energy position on the semiconductor surface.

Mallick et al. [94, 95] reported on ultralow noise MWIR InAs/GaSb SLS avalanche photodiode (APD, $\lambda_{100\%\ \text{cut-off}}$ = 4.14 µm at 77 K) passivated with ZnS. ZnS passivated APD showed a maximum R_0A value of 7.5×10^5 Ω cm^2 and dark current of 2 µA at a reverse bias of −1.0 V. Compared to an unpassivated diode, the ZnS-passivated APD demonstrated the R_0A value enhanced by a factor of 3.5, dark current reduced by an order of magnitude, as well as increased the breakdown voltage and multiplication gain by 10 V and factor of 20, respectively.

The same research group investigated the effectiveness of ZnS passivation on InAs/GaSb SLS LWIR ($\lambda_{100\%\ \text{cut-off}}$ = 10 µm at 77 K) detectors [96]. The maximum R_0A value and dark current density of ZnS passivated detector were 492 Ω cm^2 and 0.01 A/cm^2 compared to the 0.72 Ω cm^2 and 1.93 A/cm^2 of unpassivated device (Fig. 21). To reduce the native oxides, prior the deposition of ZnS the APD and LWIR detector samples were treated with 20% warm (60 °C) aqueous solution of $(NH_4)_2S$ for 10 min.

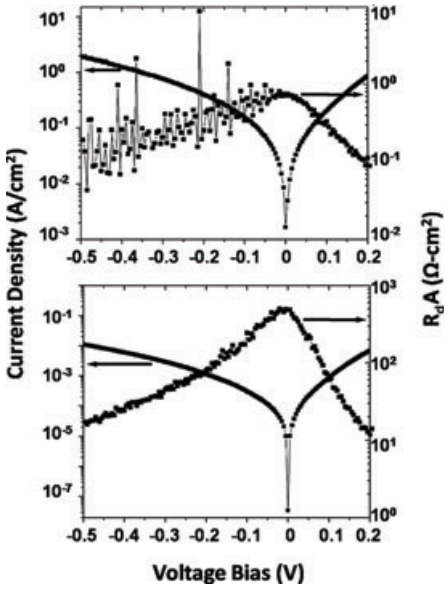

Figure 21 Dark current densities (left scale) and corresponding values of R_0A product (right scale) at different bias values for unpassivated (top) and ZnS passivated (bottom) InAs/GaSb SLS LWIR detector. Reprinted from [96].

Performance improvement of InAs/GaSb LWIR SLS detectors after ZnS passivation was also observed by Plis et al. [37]. However, dark current density for passivated detectors was reduced only by factor of 3, that may be the result of the inferior quality of deposited ZnS film.

6. Conclusion

The third generation of IR detection systems is expected to provide enhanced capabilities like larger number of pix-

els, higher frame rates, better thermal resolution as well as multicolor functionality. Type II InAs/GaSb SLSs have emerged as a promising candidate for the third generation IR detectors alternative to HgCdTe and quantum-well infrared (QWIP) technologies. One of the most demanding challenges of present day SLS technology is the suppression of surface leakage currents associated with the exposed mesa sidewalls, which appear during the definition of device optical area. With scaling of pixel dimensions to 20 μm × 20 μm, FPA performance is strongly dependent on surface effects due to large pixels' surface/volume ratio.

In this paper, we describe in detail various techniques for passivation of InAs/GaSb SLS detectors with operation wavelengths mainly covering MWIR and LWIR spectral regions. Since passivation treatment applied on rough or contaminated by native oxides or foreign particles surface will result in little or no improvement of device performance, we discussed methods of native oxide reduction and single pixel isolation. In order to reduce surface currents on InAs/GaSb SLS detectors researchers have employed encapsulation of etched sidewalls with thick layers of dielectrics (e.g. SiO_2), organic materials (polyimide and various photoresists), or wider-band gap III-V material overgrowth with wide band gap material or "shallow etch" technique) and chalcogenide passivation, that is saturation of unsatisfied bonds on semiconductor surface by S-atoms.

The dielectric passivation presents the challenges of developing high-quality, low fixed and interfacial charges density dielectrics at process temperatures substantially lower that the InAs/GaSb SLS growth temperature to prevent the SLS period intermixing. Dielectric passivation is shown to be effective for MWIR detectors; however it may not passivate the low band gap materials as effectively. The narrow bandgap devices (with bandgap of 120 eV or lower) are more susceptible to the formation of charge conduction channels along the sidewalls. Native fixed charges presented in dielectric passivation layer (e.g. SiO_2) can deteriorate the LWIR device performance. Method of band-bending control at SLS-SiO2 interface by applying a voltage along devices sidewall has been recently proposed. The ability to establish the flat-band condition at SLS-dielectric interface together with compatibility with SLS FPA fabrication procedure makes dielectric passivation very attractive for passivation of LWIR SLS detectors.

MBE re-growth of a lattice-matched wide-bandgap III-V semiconductor layer on top of the exposed mesa sidewalls of narrow-bandgap SLS detector is an elegant solution of passivation problem in LWIR wavelength range. In addition to surface current reduction due to elimination of sidewalls, reduction of SRH and Auger recombination currents is expected (for the overgrowth with GaSb). However, this passivation technique requires very careful surface cleaning prior the overgrowth procedure, which significantly complicates the fabrication process of detectors and FPAs. The shallow etch mesa isolation approach (SEMI technique) restricts the exposed surfaces to the wide-band gap layers, thus suppressing the surface recombination and the ability of surface electric fields to produce conducting channels that would bypass the junction. Since no cross-talk has been registered for LWIR FPA mini-arrays (256 × 256) fabricated with SEMI technique, this passivation approach may be a way to solve passivation of SLS detectors operating in LWIR region.

Chalcogenide passivation through an immersion in a sulfur-containing solution, or deposition of a sulfur based layer, effectively reduces dark currents in MWIR, LWIR and VLWIR InAs/GaSb SLS detectors. However, the chalcogen-based passivation does not provide physical protection and encapsulation of the device and there are some reports on the temporal instability of such a passivation layer. Additional research on appropriate encapsulation of sulfur passivation layer needs to be performed, as well as the compatibility of S-based passivation with FPA fabrication procedure still needs to be investigated. The ZnS passivation solves the task of chemical passivation (i.e. saturates the dangling bonds) and simultaneously provides protection of devices sidewalls. However, no data are available yet on LWIR FPA passivation with ZnS.

In conclusion, there are various passivation techniques developed for passivation of MWIR and LWIR InAs/GaSb SLS detectors. However, there is no universal approach developed yet that would treat equally efficiently the SLS detectors with different cut-off wavelengths. Moreover, more studies have to be conducted on long-term stability of proposed passivation schemes. Finally, since passivation needs to be successfully integrated into FPA fabrication procedure, more research on compatibility of various passivations, especially S-based, with FPA fabrication, has to be performed.

Acknowledgements. The authors would like to acknowledge support from AFOSR FA-9550-10-1-0113 and AFOSR 9550-09-1-0231 grants.

Received: 9 June 2011, **Revised:** 22 January 2012, **Accepted:** 31 January 2012

Published online: 20 March 2012

Key words: InAs/GaSb, strained layer superlattice, infrared detection, passivation.

Elena Plis is a Research Assistant Professor in Electrical and Computer Engineering Department at the Center for High Technology Materials at University of New Mexico. She received her MS/PhD degrees from University of New Mexico in 2005 and 2007, respectively, and has an engineering degree from the Kovrov State Technological Academy, Russia. Her present research interests include growth, fabrication, and characterization of type-II InAs/(In,Ga)Sb-strained layer superlattice (SLS) IR detectors for MWIR and LWIR spectral regions. She is also interested in chemistry of GaSb-based materials and possible biomedical applications of infrared detectors, such as early detection of skin cancer.

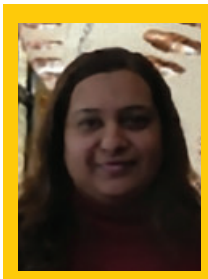

Maya Narayanan Kutty received her B.E in Electronics and Communication Engineering from Bangalore University, Karnataka, India in 2001 and her M.S. degree in Electrical Engineering from University of New Mexico, Albuquerque, NM, in 2007. She is currently pursuing her PhD at University of New Mexico. Her research interests include fabrication of opto/bio-electronic devices incorporating highly mismatched III-Vs, quantum dots, silicon and organic polymers.

Sanjay Krishna is a Professor of Electrical and Computer Engineering and the Associate Director of University of New Mexico's (UNM) Center for High Technology Materials. Dr. Krishna earned his PhD and master's degrees in electrical engineering at the University of Michigan at Ann Arbor in 2001. He holds two masters degrees, Masters of Science in Electrical Engineering from University of Michigan in 1999, and Master of Science in Physics from the Indian Institute of Technology in Madras in 1996. His research interests are the fundamental studies of physics, epitaxial growth, device fabrication and characterization.

References

[1] G. A. Sai-Halasz, R. Tsu, and L. Esaki, Appl. Phys. Lett. **30**, 651 (1977).
[2] L. Esaki, J. Cryst. Growth **52**, 227 (1981).
[3] D.L. Smith and C. Mailhiot, J. Appl. Phys. **62**, 2545 (1987).
[4] R. H. Miles, D. H. Chow, J. N. Schulman, and T. C. McGill, Appl. Phys. Lett. **57**, 801 (1990).
[5] R. Rehm, M. Walther, J. Schmitz, J. Fleibner, S. Kopta, F. Fuchs, W. Cabanski, and J. Ziegler, J. Cryst. Growth **278**, 150 (2005).
[6] Y. Wei, A. Hood, H. Yau, A. Gin, M. Razeghi, M. Z. Tidrow, and V. Nathan, Appl. Phys. Lett. **86**, 233106 (2005).
[7] E. Plis, J. B. Rodriguez, H. S. Kim, G. Bishop, Y. D. Sharma, L. R. Dawson, S. Krishna, S. J. Lee, C. E. Jones, and V. Gopal, Appl Phys. Lett. **91**, 133512 (2007).
[8] I. Vurgaftman, E. Aifer, C. Canedy, J. Tischler, J. Meyer, J. Warner, E. Jackson, G. Hildebrandt, and G. Sullivan, Appl. Phys. Lett. **89**, 121114 (2006).
[9] D. Z. Y. Ting, C. J. Hill, A. Soibel, S. A. Keo, J. M. Mumolo, J. Nguyen, and S. D. Gunapala, Appl. Phys. Lett. **95**, 023508 (2009).
[10] S. D. Gunapala, D. Z. Ting, C. J. Hill, J. Nguyen, A. Soibel, S. B. Rafol, S. A. Keo, J. M. Mumolo, M. C. Lee, J. K. Liu, and B. Yang, IEEE Photon. Tech. Lett. **22**, 1856 (2010).
[11] N. Gautam, H. S. Kim, M. N. Kutty, E. Plis, L. R. Dawson, and S. Krishna, Appl. Phys. Lett. **96**, 231107 (2010).
[12] P. Y. Delaunay and M. Razeghi, IEEE J Quant Electron **46**, 584 (2010).
[13] Y. Wei, A.Gin, M. Razeghi, and G. J. Brown, Appl. Phys. Lett. **81**, 3675 (2002).
[14] A. Hood, M. Razeghi, E. Aifer, and G. Brown, Appl. Phys. Lett. **87**, 151113 (2005).
[15] J. Rothman, E. D. Borniol, P. Ballet, l. Mollard, S. Gout, M. Fournier, J. P. Chamonal, G. Destefanis, F. Pistone, S. Courtas, X. Lefoule, and P. Tribolet, Proc. of SPIE **7298**, 729835 (2009).
[16] J. Peterson, D. Lofgreen, J. Franklin, T. Vang, E. Smith, J. Wehner, I. Kasai, J. Bangs, S. Johnson, and M. Reddy, J. Electron. Mater. **37**(9), 1274 (2008).
[17] I. Pivnik, E. Ilan, A. Calalhorra, A. Koifman, I. Vaserman, J. O. Schlesinger, R. Gazit, and I. Hirsh, Proc. of SPIE **7298**, 72983K-1 (2009).
[18] A. Rogalski, Rep. Progr. Phys. **68**, 2267 (2005).
[19] H. Schneider and H. C. Liu, Quantum Well Infrared Photodetectors, Springer Series in Optical Sciences (Springer, Berlin, Germany, 2007).
[20] A. Soibel, S. V. Bandara, D. Ting, J. K. Liu, J. Mumolo, S. B. Rafola, W. Johnson, D. Wilson, and S. Gunapala, Inf. Phys. Technol. **52**(6), 403 (2009).
[21] A. Nedelcu, V. Gueriaux, A. Bazin, L.Dua, A. Berurier, E. Costard, P. Bois, and X. Marcadet, Inf. Phys. Technol. **52**(6), 412 (2009).
[22] M. Walther, R. Rehm, J. Schmitz, F. Rutz, J. Fleissner, and J. Ziegler, Proc. of SPIE **6940**, 6940A-1 (2008).
[23] E. R. Youngdale, J. R. Meyer, C. A. Hoffman, F. J. Bartoli, C. H. Grein, P. M. Young, H. Ehrenreich, R. H. Miles, and D. H. Chow, Appl. Phys. Lett. **64**, 3160 (1994).
[24] C. H. Grein, M. E. Flatte, H. Ehrenreich, and R. H. Miles, J. Appl. Phys. **77**, 4153 (1995).
[25] C. Grein, H. Cruz, M. Flatte, and H. Ehrenreich, Appl. Phys. Lett. **65**, 2530 (1994).
[26] M. Kinch, J. Electron. Mater. **29**, 809 (2000).
[27] A. Rogalski, Opt. Eng. **42**(12), 3498 (2003).
[28] A. Rogalski, Prog. Quantum Electron. **27**, 59 (2003).
[29] A. Rogalski, New Ternary Alloy systems for Infrared Detectors (SPIE, Bellingham, Washington, 1994).
[30] A. Ongstad, R. Kaspi, C. Moeller, M. Tilton, D. Gianardi, J. Chavez, and G. Dente, J. Appl. Phys. **89**, 2185 (2001).
[31] J. Steinshnider, M. Weimer, R. Kaspi, and G. W. Turner, Phys. Rev. Lett. **85**, 2953 (2000).
[32] G. J. Brown, Proc. of SPIE **5783**, 65 (2005).
[33] K. Banerjee, S. Ghosh, E. Plis, and S. Krishna, J. Electron. Mater. **39**, 2210 (2010).
[34] G. P. Schwartz, Thin Solid Films **103**, 3 (1983).
[35] T.Wada and N.Kitamura, J. J. Appl. Phys. **27**(4), 686 (1988).
[36] G. Hollinger, R. Skheyta-Kabbani, and M. Gendry, Phys. Rev. B **49**, 11159 (1994).
[37] E. Plis, M. N. Kutty, S. Myers, H. S. Kim, N. Gautam, L. R. Dawson, and S. Krishna, Inf. Phys. Technol. **54**, 252 (2010).
[38] A. Gin, Y. Wei, J. Bae, A. Hood, J. Nah, and M. Razeghi, Thin Solid Films **447–448**, 489 (2004).
[39] R. Rehm, M. Walther, J. Schmitz, J. Fleibner, F. Fuchs, J. Ziegler, and W. Cabanski, Opt.-Electron. Rev. **14**, 19 (2006).
[40] E. K. Huang, B. M. Nguyen, D. Hoffman, P. Y. Delaunay, and M. Razeghi, Proc. of SPIE **7222**, 72220Z–72220Z–08 (2009).
[41] J. W. Lee, W. T. Lim, I. K. Baek, S. R. Yoo, M. H. Jeon, G. S. Cho, and S. J. Peatron, J. Electron. Mater. **33**, 358 (2004).
[42] E. K. W. Huang, S. Hoffman, B. M. Nguyen, P. Y. Delaunay, and M. Razeghi, Appl. Phys. Lett. **94**, 053506 (2009).
[43] R. Rehm, M. Walther, F. Fuchs, J. Schmitz, and J. Fleissner, Appl. Phys. Lett. **86**, 173501 (2005).
[44] B. M. Nguyen, D. Hoffman, E. K. Huang, P. Y. Delaunay, and M. Razeghi, Appl. Phys. Lett. **93**, 123502 (2006).

[45] R. Chaghi, C. Cervera, H. Ait-Kaci, P. Grech, J. B. Rodriguez, and P. Christol, Semicond. Sci. Technol. **24**, 065010 (2009).
[46] C. Cervera, J. B. Rodriguez, R. Chaghi, H. Ait-Kaci, and P. Christol, J. Appl. Phys. **160**, 024501 (2009).
[47] Y. Chen, A. Moy, S. Xin, K. Mi, and P. P. Chow, Inf. Phys. Technol. **52**, 340 (2009).
[48] S. dip Das, S. L. Tan, S. Zhang, Y. L. Goh, C. H. Ting, and J. David, in: Proceedings of the 6th EMRS DTC Technical Conference, Edinburgh 2009, p. B7.
[49] M. N. Kutty, E. Plis, A. Khoshakhlagh, N. Gautam, S. Smolev, Y. D. Sharma, R. L. Dawson, S. Krishna, S. J. Lee, and S. K. Noh, J. Electron. Mater. **39**, 2203 (2010).
[50] E. R. Weber, in: Advances in Infrared Photodetectors, edited by S. Gunapala, D. Rhiger, and C. Jagadish, Semiconductors and Semimetals Vol. 84 (Elsevier, San Diego, CA, USA, 2010), p. 38.
[51] M. Sundaram, A. Reisinger, R. Dennis, K. Patnaude, D. Burrows, J. Bundas, K. Beech, and R. Faska, Inf. Phys. Technol. **54**, 243 (2011).
[52] J. Nguyen, A. Soibel, D. Z. Y. Ting, C. J. Hill, M. C. Lee, and S. D. Gunapala, Appl Phys. Lett. **97**, 051108 (2009).
[53] V. N. Bessolov and M. V. Lebedev, Semiconductors **32**, 1141 (1998).
[54] V. Gopal, Semicond. Sci. Technol **11**, 1070 (1994).
[55] Y. T. Kim, D. S. Kim, and D. H. Yoon, Thin Solid Films **475**, 271 (2005).
[56] J. A. Nolde, R. Stine, E. M. Jackson, C. L. Canedy, I. Vurgaftman, S. I. Maximenko, C. A. Affouda, M. Gonzalez, E. H. Aifer, and J. R. Meyer, Proc. of SPIE **7945**, 79451Y-1 (2011).
[57] G. Chen, B. M. Nguyen, A. M. Hoang, E. K. Huang, S. R. Darvish, and M. Razeghi, Appl. Phys. Lett. **99**, 183503-1 (2011).
[58] B. M. Nguyen, D. Hoffman, E. K. Huang, P. Y. Delaunay, and M. Razeghi, Appl. Phys. Lett. **93**, 123502 (2008).
[59] P. Y. Delaunay, A. Hood, B. M. Nguyen, D. Hoffman, Y. Wei, and M. Razeghi, Appl. Phys. Lett. **91**, 091112 (2007).
[60] H. S. Kim, E. Plis, A. Khoshakhlagh, S. Myers, N. Gautam, Y. D. Sharma, L. R. Dawson, S. Krishna, S. J. Lee, and S. K. Noh, Appl. Phys. Lett. **96**, 033502 (2010).
[61] J. E. A. DeCuir, J. W. Little, and N. Baril, Proc. of SPIE **8155**, 815508-1 (2011).
[62] H. S. Kim, E. Plis, N. Gautam, S. Myers, Y. Sharma, L. R. Dawson, and S. Krishna, Appl Phys. Lett. **97**, 143512 (2010).
[63] US Patent No. 4882245, 1989.
[64] A. Agirregabiria, F. J. Blanco, J. Berganzo, M. T. Arroyo, A. Fullaondo, K. Mayora, and J. M. Ruano-Lopez, Lab on a Chip **5**, 545 (2005).
[65] Y. Qian, S. Kim, J. Song, and G. P. Nordin, Opt. Express **14**, 6020 (2006).
[66] M. Shaw, D. Nawrocki, R. Hurditch, and D. Johnson, Microsyst. Technol. **10**, 1 (2003).
[67] A. Hood, P. Y. Delaunay, D. Hoffman, B. M. Nguyen, Y. Wei, and M. Razeghi, Appl Phys. Lett. **90**, 233513 (2007).
[68] F. Szmulowicz and G. J. Brown, Inf. Phys. Technol. **53**, 305 (2011).
[69] E. H. Aifer, J. H. Warner, C. L. Canedy, I. Vurgaftman, E. M. Jackson, J. G. Tischler, J. R. Meyer, S. P. Powell, K. Olver, and W. E. Tennant, J. Electron. Mater. **39**, 1070 (2010).
[70] C. J. Sandroff, M. S. Hegde, and C. C. Chang, J. Vac. Sci. Technol. B **7**, 841 (1989).
[71] C. J. Spindt, D. Liu, K. Miyano, P. L. Meissner, T. T. Chiang, T. Kendelewicz, I. Lindau, and W. E. Spicer, Appl. Phys. Lett. **55**, 861 (1989).
[72] V. Bessolov, E. Konenkova, and M. Lebedev, Mater. Sci. Eng. B **44**, 376 (1997).
[73] D. Paget, A. O. Gusev, and V. L. Berkovits, Phys. Rev. B **53**, 4615 (1996).
[74] H. Oigawa, J. Fan, Y. Nannichi, H. Sugahara, and M. Oshima, Jap. J. Appl. Phys. **30**, L322-1 (1991).
[75] D. Petrovykh, M. Yang, and L. Whitman, Surf. Sci. **523**, 231 (2003).
[76] M. Perotin, P. Coudray, L. Gouskov, H. Luquet, C. Linares, J. Bonnet, L. Soonckindt, and B. Lambert, J. Electron. Mater. **23**, 7 (1994).
[77] P. S. Dutta, K. S. Sangunni, H. L. Bhat, and V. Kumar, Appl. Phys. Lett. **65**, 1695 (1994).
[78] S. Basu and P. Barman, J. Vac. Sci. Technol. B **10**(3), 1078 (1992).
[79] V. N. Bessolov, M. V. Lebedev, E. B. Novikov, and B. V. Tsarenkov, J. Vac. Sci.Technol. B **11**, 10 (1993).
[80] V. N. Bessolov, Y. V. Zhilyaev, E. V. Konenkova, and M. V. Lebedev, J. Tech. Phys. **43**, 983 (1998).
[81] T. Ohno, Surf. Sci. **225**, 229 (1991).
[82] T. Ohno and K. Shiraishi, Phys. Rev. B **42**, 11194 (1990).
[83] Z. Y. Liu, T. F. Kuech, and D. A. Saulys, Appl. Phys. Lett. **83**, 2587 (2003).
[84] Z. Y. Liu, A. A. Gokhale, M. Mavrikakis, D. A. Saulys, and T. F. Kuech, J. Appl. Phys. **96**, 4302 (2004).
[85] Z. Y. Liu, B. Hawkins, and T. F. Kuech, J. Vac. Sci. Technol. B **21**, 71 (2003).
[86] A. Gin, Y. Wei, A. Hood, A. Bajowala, V. Yazdanpanah, M. Razeghi, and M. Tidrow, Appl. Phys. Lett. **84**, 2037 (2004).
[87] Nist X-ray photoelectron spectroscopy database, version 3.5, http://srdata.nist.gov/xps/ (2003), date of last visit: 17 January 2012.
[88] M. R. Ravi, A. DasGupta, and N. DasGupta, J. Cryst. Growth **268**, 359 (2004).
[89] R. Stine, E. H. Aifer, L. J. Whitman, and D. Y. Petrovykh, Appl. Surf. Sci. **255**, 7121 (2009).
[90] A. Salesse, A. Joullie, P. Calas, J. Nieto, F. Chevrier, Y. Cuminal, G. Ferblantier, and P. Christol, Phys Stat Solidi (c) **4**, 1508 (2007).
[91] K. Banerjee, J. Huang, S. Ghosh, R. Xu, C. G. Takoudis, E. Plis, S. Krishna, S. Ketharanathan, and M. Chriss, Proc. of SPIE **8012**, 801243 (2011).
[92] E. Plis, J. B. Rodriguez, S. J. Lee, and S. Krishna, Electron. Lett. **42**, 1248 (2006).
[93] S. H. Lee, S. H. Bae, H. C. Lee, and C. K. Kim, J. Electron. Mater. **27**, 684 (1998).
[94] S. Mallick, K. Banerjee, S. Ghosh, E. Plis, J. B. Rodriguez, S. Krishna, and C. Grein, Appl. Phys. Lett. **91**, 241111 (2007).
[95] S. Mallick, K. Banerjee, S. Ghosh, J. B. Rodriguez, and S. Krishna, IEEE Photon. Tech. Lett. **19**, 1843 (2007).
[96] K. Banerjee, S. Ghosh, S. Mallick, E. Plis, and S. Krishna, J. Electron. Mater. **38**, 1944 (2009).